Advances in Water Resources 159 (2022) 104058

Contents lists available at ScienceDirect

Advances in Water Resources

journal homepage: www.elsevier.com/locate/advwatres

An accurate reduced-dimension numerical model for evolution of electrical potential and ionic concentration distributions in a nano-scale thin aqueous film

Sona Aseyednezhad [a,b], Lifei Yan [a], S. Majid Hassanizadeh [a,c], Amir Raoof [a,*]

[a] Environmental Hydrogeology Group, Department of Earth Sciences, Utrecht University, Utrecht 3584 CB, the Netherlands
[b] Department of Energy, Politecnico di Milano, Italy
[c] Center of Excellence for Simulation Technology, Stuttgart University, Germany

ARTICLE INFO

Keywords:
Thin film hydrodynamics
Electrochemical potential
Charged surface
Coupled process
Poisson-Nernst-Planck equations

ABSTRACT

The numerical modelling of ionic diffusive transport through a charged thin film of electrolyte is mathematically and computationally complex due to the strongly coupled hydrodynamics and electrochemical interactions. Generally, simulations are performed by solving the Poisson equation together with the Nernst-Planck flux formula to model electrochemical processes in electro-diffusion problems. One important application of these system of equations to study the interaction of ionic diffusion and thin film hydrodynamics in petroleum engineering. However, due to the highly nonlinear and coupled equations the computational costs are heavy and very often limited to simulations in two-dimensional geometries. In this article, we have developed an equivalent one-dimensional electro-diffusive transport model based on mathematical averaging of 2D equations to reduce the computational time. Doing so, the computational time is improved substantially and simulation of much larger domain sizes which are required to study and interpret the experimental results is shown to be feasible. We have shown the high accuracy of the developed model by comparing the electric potential and concentration profiles of the developed model against the original 2D simulations. The developed approach reduces the computational effort by over 200 times without losing accuracy.

1. Introduction

Poisson-Nernst-Planck (PNP) equations are widely used to describe transport of ions in various applications including chemistry, physics, biology, and engineering (Suopaiarvi, 2015; Bazant et al., 2009; Eisenberg, 1998; Kurnikova et al., 1999; Selberherr, 1984). Poisson equation is used to describe the electrical potential and the Nernst-Planck equation is applied to include the electric double layer effects in the transport of ions through a thin layer of electrolyte. Applying PNP equations in numerical modelling with application to membrane electrochemistry dates back to 1975 in the work of Cohen and Cooley and that of Brumleve and Buck (Cohen and Cooley, 1965; Brumleve and Buck, 1978). Use of PNP equations allows the computation of the space charge density near an interface which may represent a solution/electrode or solution/ion-exchange membrane interface (Uzdenova et al., 2018). In addition, PNP equations are also known as the drift-diffusion equations and are used for simulating ion diffusion in semiconductor devices (Markowich, 1986; Rouston, 1990; Newman, 1991). In these systems, the diffusion of ions is affected by the excess chemical potential produced by the mobile ions. Another application of PNP equations is in biological membrane channels (Ardenas et al., 2000; Hollerbach et al., 2000; Coalson and Kurnikova, 2005) where the underlying mechanisms for ion transport through such channels are studied to understand the cellular activities of the living cells (Eisenman and Dani, 1987; Hille, 1978). Moreover, the PNP equations have been applied for solving ion transport in general nano- to macro-scale charged porous media (Pivonka et al., 2009; Mohajeri et al., 2010). They can be also applied for describing special mechanisms behind the flow and transport behaviors in unconventional reservoirs. In these systems, the widespread nanopores are often considered as the main cause of significant capillary and confinement effects. Zhang et al. (2020) designed a digital twin platform by which they combined several promising numerical models and multiscale algorithms. Their model approach covered all the effects of capillarity, sorption and salinity to simulate and illustrate the effect of

* Corresponding author.
E-mail address: a.raoof@uu.nl (A. Raoof).

https://doi.org/10.1016/j.advwatres.2021.104058
Received 12 July 2021; Received in revised form 12 October 2021; Accepted 13 October 2021
Available online 16 October 2021

these mechanisms on flow and transport phenomena and the production of unconventional reservoirs. They mentioned water salinity as one of the key factors affecting injection and fracturing performance. For the two directly relevant processes to salinity, they used multicomponent ion exchange equation and DLVO theory to represent the electrical interaction process and the double-layer expansion, respectively. The Poisson-Boltzmann equation was used to model electrostatic double-layer force and the effect of dynamic sorption was represented by the Nernst-Planck equation. Moreover, numerous studies on unconventional oil and gas production indicate that under confinement the fluid behavior deviates from its bulk behavior (Alharthy et al., 2013; Chen et al., 2013; Du and Chu, 2012). Thus, phase behavior modelling becomes significant as the change of reservoir fluid properties could affect the flow mechanisms and displacement processes. Since the nano-scale pore yields a large capillary pressure, capillary effect should be considered in modelling phase behaviors in unconventional reservoirs (Sun, 2019). In this regard, a well-developed flash calculation scheme which is stablished at fixed chemical composition (N), volume (V) and temperature (T), known as NVT flash, was established by Zhang et al. (2020). Their trained model was capable of accurately estimating the phase behavior of complex reservoir fluids under a wide range of environmental conditions, in the presence of capillary pressure. For electrically charged nano-porous materials, such as electrodes, the formation of electrical double layer (EDL) considerably influences the transport and electro-sorption of ions inside the nanopores. This phenomenon leads to changes in pore accessibility (Zhang and Tartakovsky; 2017). Damiani et al. (2021) developed a reactive transport model based on the PNP to simulate diffusion of ions through a charged constricted pore. Their work contributed to the understanding of electrochemical migration of ions caused by changes in electric fields under various chemically reactive conditions such as those related to the swelling of clay minerals. The complex composition of mineral surfaces in geological media, either chemical heterogeneity or pore property, poses challenges in accurate description of ionic transport in porous media (Naidu et al., 1994; Norde and Lyklema, 1978). For example, in simulation of electrokinetic processes in fluid saturated porous materials, ζ potential is a fundamental property for charged surfaces that represents approximately the electrical potential at the mineral-fluid interface (Pride, 1994). Revil and Pezard (1999) considered a silica-dominated porous material filled with a binary symmetric 1:1 electrolyte, such as NaCl. They developed analytical expressions for ζ potential and the specific surface conductance and predicted the variation of these parameters with the pore fluid salinity, temperature, and pH. In the field of particle transport, Trefalt et al. (2016) discussed the effect of charge regulation in Electrical Double Layer (EDL) on the interaction between colloids and interfaces by using the classical Poisson-Boltzmann theory. Several researchers have proposed theories to explain the impact of interfacial properties on macroscopic transport (Alizadeh et al., 2019; Liu et al., 2020). Yet, an accurate simulation of electrochemical processes in the presence of dynamic changes in electrical potential and ionic concentration induced by the alteration of solid charged surfaces and the surrounding electrolyte remains a challenging task.

Considering clayey soil as a notable example of charged porous media, different studies worked on flow, ion and chemical transport, and deformation in these systems (Kirby, 2010; Mahani, 2015; Niasar and Mahani, 2016). Mahani (2015) used a model system for sandstone rock consisting of clay minerals deposited at the glass substrate and oil droplets which were attached to clay patches separately. Their study was under the assumption of hydrodynamic equilibrium between the oil phase and the surrounding water. They studied ion diffusion and transport when the system is exposed to two different brine solutions having low and high salinity values. Later, they studied the DLVO intermolecular forces by considering electrostatic forces and including osmotic pressure to understand the dynamics of disjoining pressure inside a thin film of electrolyte (Niasar and Mahani, 2016). They coupled the Nernst-Planck ionic transport and Poisson equations with Navier-Stokes equation in order to describe the disjoining pressure and investigate its impact on the transport of ions within the thin film. They found that the nonlinear behaviour in the pressure field, which is caused by multidirectional and asymmetric ions transport, is strongly affected by the diffusion length and the overlapping of EDL.

While the coupled PNP model provides quantitative prediction of ion transport problem in many areas, it has its own limitations such as neglecting the finite size effect of ion particles and correlation effect (i.e., self-energy) which may become important in very confined channels (Jung et al., 2009).

Concerning model limitations such as ion-ion interactions and steric effects, some recent theoretical modifications have been proposed. For example, Corry et al. (2003) demonstrated that if a specific self-energy term is included in the NP equation, qualitative improvements could be made in the computational results. Kilic et al. (2007) proposed a simple modification of the widely used PNP equations through including the steric effect due to ion transport. They reported that some limitations confronted in specific applications, such as those related to ionic channels, can be sufficiently improved by adjusting the diffusion coefficients, or by considering additional force terms in the ion flux formula of the NP equation (Zheng and Wei, 2011).

On the other hand, one of the challenges in the application of PNP to model ion transport in electrode and membrane system is the implementation of certain boundary conditions that make models mathematically complex. For example, this is encountered in 2D modelling of ion and water transfer to describe electrochemical processes in membranes (Pismensky et al., 2012) and electrodes in galvanostatic mode (Mareev et al., 2016) on the basis of local electroneutrality. This required applying an integral boundary condition for the electric current density which caused high computational demands. Uzdenova et al. (2018) proposed a 1D model based on PNP equations for the galvanostatic mode. Their model eliminated the need for an additional interface for the time integral calculations. They specified the electric potential gradient as an explicit function of the total current density at the outer edge of the diffusion layer of ion-exchange membrane /solution interface instead of the time derivative of the electric potential gradient at this boundary. Their model eliminated the need for an additional coupling due to the time integral calculations.

Other importance of simplifying the numerical models based on PNP equations is related to the fact that they are computationally very complex. For example, to improve the computational efficiency in the study of ion transport in a multilayer graphene membrane, one approach would be to reduce the dimensionality of the nanochannel. Doing so, the computational cost of the problem without significant loss of accuracy are significantly reduced. Jiang et al. (2014) have developed an equivalent one-dimensional ion transport model for the tortuous nano-slit systems embedded in a multi-layered graphene membrane. They concluded that the equivalent 1D model should provide a framework to interpret and rationalize the experimental results of ion transport in the cascading nano-slit systems. It may provide a simple, yet quantitative, model to design 2D materials-based membranes for various applications, such as energy storage, electrode design, ion separation, water desalination or treatment.

The aim of this study is to enhance the computational efficiency needed to simulate ion transport in charged media. We have first developed a 2D axi-symmetric model to investigate the ion transport within a film of water underlying an oil droplet, with negatively charged surfaces on its top and bottom boundaries. The liquid film is initially composed of a high salinity electrolyte, and, afterwards, it is exposed through its lateral sides to a bulk fluid with a lower salinity. This contact initiates a dynamic process with diffusion of ions and the subsequent evolution of the electric field over time across the liquid film.

Our 2D model was developed based on the model proposed by Mahani et. al 2016 in which the interaction of ionic diffusion and thin film hydrodynamic was studied. In simulations using the developed 2D model, only very small domain size could be considered as otherwise the

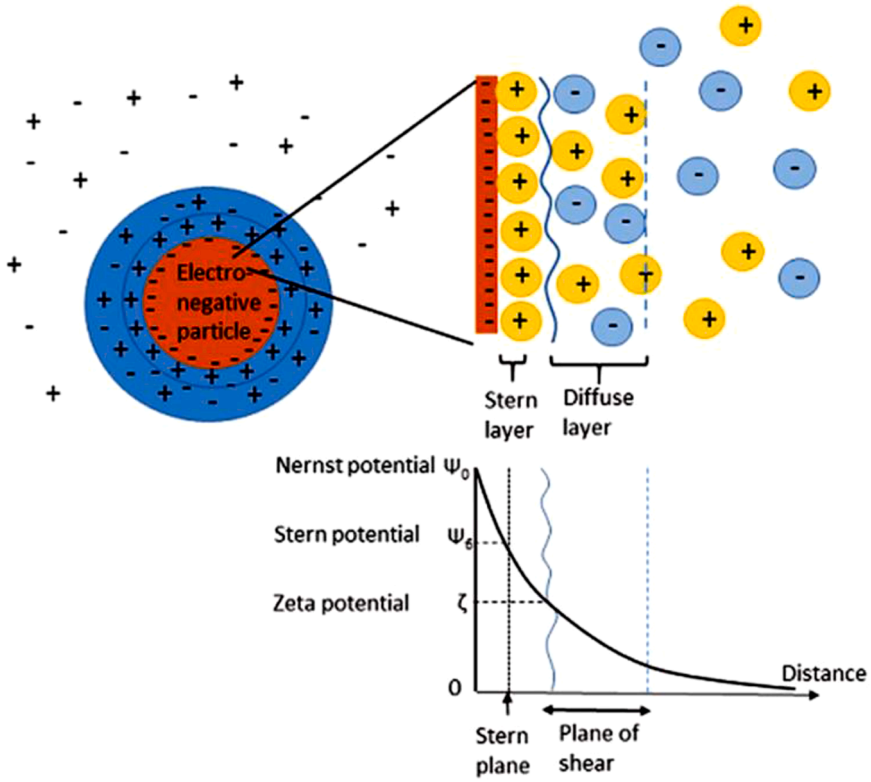

Fig. 1. Schematic of an electric double layer (EDL) and electrical charge distribution near a negatively charged surface (Kelessidis, 2021).

very large domain aspect ratio could cause numerical problems. Considering the assumptions of fixed and rigid boundaries and incompressible water phase in the 2D model, there is no net inflow of water into the domain. There could be flow circulation within the domain which is expected to be very small. In a next step, in order to reduce the complexity and the computational effort, we have derived and developed an averaged, one-dimensional, coupled Poisson-Nernst-Plank model to simulate electro-diffusion in the same system. To do so, we have integrated the governing differential equations along the channel height. This strategy allowed us to solve the equations for a much larger realistic domain size relative to that used in the 2D model. The COMSOL Multiphysics software was used to solve the coupled PNP equations in our 1D and 2D models. Our results using the 1D model showed exact agreement with the results from the 2D model, but with significantly less computational time and modelling complexity.

2. Theory

In this section, we will describe the Electrical Double Layer (EDL) and the general form of the equations used in this study to simulate the electric field and ion transport within the channel.

2.1. EDL

As you can see in Fig. 1, an EDL has a structure of two parallel layers of charges appearing at the surface of a material when exposed to an ionic solution.

The first layer, called stern layer, consists of either positive or negative ions adsorbed onto the surface due to chemical interactions. The second layer is formed by ions attracted to the surface charge via the coulomb force (shear plane) and free ions moving in the fluid under the influence of electric attraction and thermal motion (diffuse layer). Typically, the electric double layer may be of interest when modelling very thin layers of electrolyte such as that studied here. To model the behaviour of the diffuse double layer, one should solve Nernst-Plank equations for all ions in combination with the Poisson equation for the electrical potential.

2.2. Electric Field

To simulate the electric field, we use the coupled Poisson-Nernst Plank (PNP) equations. The electro-osmotic flow occurs through the film because electric double-layers are developed at the top and bottom interfaces and overlap with each other. Under these conditions, there is no thermodynamic equilibrium and thus Poisson-Boltzmann equations cannot be used for the simulation of ionic distribution. Instead, the Nernst-Planck equation should be used to find the distribution of ions within the electric double-layer (Park et al., 2007) under dynamic non-equilibrium condition. To model the electrical potential, the Poisson equation is used as:

$$\nabla^2\Psi = -\frac{\rho_e}{\varepsilon} \tag{1}$$

where ε is the permittivity of the medium and ρ_e is the charge density due to ion concentrations. The latter can be described as:

$$\rho_e = \sum e z_i n_a c_i \tag{2}$$

where c_i, represents concentrations of two ions of opposite charge, z_i, n_a and e denote the valence of the ion i (+1/ -1), Avogadro number and elementary charge, respectively.

2.3. Ion Transport

To solve for the concentrations, c_i, of two ions in an electrolyte solution, we can use the Nernst-Planck equation. The molar flux of ions, j_i, are described as follow:

$$j_i = c_i V - D_i \nabla c_i - u_{m,i} z_i F c_i \nabla\Psi \tag{3}$$

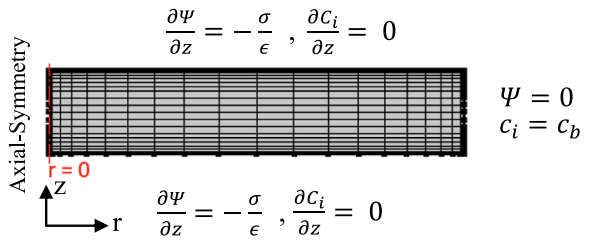

Fig. 2. The 2D representations of the simulation domain together with the boundary conditions for Poisson and Nernst-Planck Equations. The domain in 2D represents a radial cross section of 20 nm long with a total height of 4 nm ($L = 20nmandh = 4nm$). The left boundary is axisymmetric, and the right boundary applies a zero electric potential and a fixed concentration of bulk solution. The top and bottom boundaries represent negatively charged surfaces are the interfaces of electrolyte with oil and clay, respectively, and carrying constant surface charge density and no-mass-flux conditions.

where D_i is the diffusion coefficient, V is advective velocity, $u_{m,i}$ is the mobility, F is Faraday's constant, and Ψ is the electrical potential. The conservation of ions in a medium provides $\frac{\partial c_i}{\partial t} + (\nabla . j_i + R_i) = 0$. Assuming no chemical reactions ($R_i = 0$) in the electrolyte, for the two species under equilibrium and dynamic condition we obtain, respectively:

$$\nabla . j_i = 0 \tag{4}$$

$$\frac{\partial c_i}{\partial t} + \nabla . j_i = 0 \tag{5}$$

3. Numerical modelling

3.1. Modelling approach and model configurations

In this study, we assumed that a thin layer of high salinity electrolyte solution is squeezed between an oil droplet and a clay platelet and is initially under thermodynamically equilibrium condition. Then, we exposed the lateral boundaries of the domain with a solution having lower salinity. This initiates the diffusion of ions and evolution of electric field through the film. Such a thin layer can be conceptualized as a disc with axis-symmetrical properties (Mahani, 2015). To simulate electric field and ions transport within this thin layer, we first developed a 2D model. Due to the coupling between highly complex and nonlinear equations, this model had relatively heavy computational costs which limits its usage for larger realistic domain sizes because of the high aspect ratio. This problem together with the dominant flow and transport in the horizontal direction motivates developing an equivalent 1D model to reduce the computational efforts and do the simulation for larger domain which is comparable to the experiment.

3.2. 2D model

3.2.1. Initial and boundary conditions in the 2D model

In the following, a 2D simulation domain and schematic overview of the relevant boundary conditions are presented. As shown in Fig. 2, the 2D system is modelled as axisymmetric geometry with an axial coordinate z and a radial coordinate r, respectively. In finite element method, using an appropriate mesh for the system is important. We have tested several mesh sizes to find an optimum mesh size that provides stable solutions. In the 2D model, within Debye lengths of top and bottom boundaries, the minimum element size was set to $(\frac{\lambda_D^H}{6})$ and the maximum element size was set to $(\frac{\lambda_D^H}{4})$, to ensure sufficient resolution for the electric double layer. Here, λ_D^H, is the Debye length for the system under high salinity initial condition, and is determined using $\lambda_D^H = \left(\frac{\varepsilon k_B T}{e^2 n_a \sum z_i^2 c_b^H}\right)^{0.5}$.

Given the domain geometry, we have used structured meshes that provided accurate and computationally efficient results (compared to the unstructured triangular mesh) as shown in Fig. 2. In order to compare our results with those of Mahani et. al, we considered a similar film size with a radius of 20 *nm* and a height of 4 *nm* (*i.e.*, $L = 20nmandh = 4nm$). On the left boundary of the domain (i.e., the symmetry axis of the cylindrical domain) a no-flux boundary condition was imposed. At the right boundary, being exposed to the low salinity bulk solution, the electrical potential was set to zero and the concentrations of the cation and anion species, c_p and c_m (mol/m3), were set to a constant value c_b (i.e., the concentration of low salinity solution in the bulk region). The top and bottom boundaries represent the interfaces of the electrolyte with oil and clay, respectively, which are negatively charged surfaces and carry constant surface charge density, σ (c/m2), and a no-flux ($-n.D\nabla c_i = 0$) boundary conditions for Nernst-Planck equation. We specified a space charge density of $\rho_e = en_a(c_p - c_m)$ (C/m3) on the entire domain.

We assumed that initially the system is in equilibrium with residing high salinity bulk solution. To solve for the corresponding initial distribution of electrical potential $\Psi(r, z)$ and concentration field, of the cation and the anion $C_i(r,z)$ for our 2D model we solved Eq. (1) and Eq. (4), respectively. As the domain is closed with fix boundaries and water is considered incompressible, the flow into the domain is zero and there is no need to simulate fluid flow.

3.2.2. 2D cylindrical form of the governing equations under dynamic condition

In this section, we provide the governing equations for electrical potential $\Psi(r, z)$ and concentration field of cation and anion $C_i(r,z)$ in a cylindrical coordinate for our 2D model under dynamic condition. As we exposed the right boundary to the low salinity bulk solution, the diffusion of ions and evolution of electric field occurs through the film. In Poisson equation to calculate the electrical potential $\Psi(r, z)$, Eqs. (1) and (2) can be written for axi-symmetric conditions as:

$$\frac{\partial^2 \Psi}{\partial z^2} + \frac{1}{r}\frac{\partial}{\partial r}\left(r\frac{\partial \Psi}{\partial r}\right) = -\frac{\sum eN_a z_i c_i}{\varepsilon} \tag{6}$$

For ions transport under dynamic condition (and excluding the convection term) Eqs. (5) and (3) provide:

$$\frac{\partial c_i}{\partial t} + \frac{D_i}{k_B T} N_a e z_i \left[\frac{\partial}{\partial z}\left(c_i \frac{\partial \psi}{\partial z}\right) + \frac{1}{r}\frac{\partial}{\partial r}\left(c_i r \frac{\partial \psi}{\partial r}\right)\right] + D_i\left[\frac{\partial^2 c_i}{\partial z^2} + \frac{1}{r}\frac{\partial}{\partial r}\left(r\frac{\partial c_i}{\partial r}\right)\right] = 0 \tag{7}$$

3.3. 1D model

3.3.1. 1D domain and boundary conditions

The 1D model has a length of 20 nm long, representing the extent of the electrolyte between oil and clay. In this model, the left boundary is axi-symmetric, and the right boundary applies a zero electric potential and a fixed concentration of bulk solution for Poisson and Nernst-Planck Equations, respectively.

3.3.2. Derivation of the 1D form of the governing equations in the radial coordinate

In order to derive the 1D equations, we integrate all terms along the height of the film. First, we define the averaged electrical potential $\overline{\Psi}(r)$ and averaged ion concentrations $\overline{C_i}(r)$ as:

$$\overline{\Psi}(r) = \frac{1}{h}\int_0^h \Psi(r, z)dz \tag{8}$$

Table 1
This table includes the integrated forms of all terms of Poisson and Nernst-Planck equations.

Integrated form of each term of Poisson equation	
$\int_0^h \frac{\partial^2\Psi}{\partial z^2}dz = \left(\frac{\partial\Psi}{\partial z}\right)_h - \left(\frac{\partial\Psi}{\partial z}\right)_0 = -\frac{\sigma}{\varepsilon} - \frac{\sigma}{\varepsilon} = -2\frac{\sigma}{\varepsilon}$	Eq. (10)
$\int_0^h \frac{1}{r}\frac{\partial}{\partial r}\left(r\frac{\partial\Psi}{\partial r}\right)dz = \frac{1}{r}\frac{\partial}{\partial r}\left(r\frac{\partial\overline{\Psi}h}{\partial r}\right)$	Eq. (11)
$-\int_0^h \frac{\sum eN_a z_i c_i}{\varepsilon}dz = -\frac{h\sum eN_a z_i \overline{c_i}}{\varepsilon}$	Eq. (12)
Integrated form of each term of Nernst-Planck equation	
$\int_0^h \frac{\partial}{\partial z}\left(c_i\frac{\partial\Psi}{\partial z}\right)dz = \left(c_i\frac{\partial\Psi}{\partial z}\right)_h - \left(C_i\frac{\partial\Psi}{\partial z}\right)_0 = -c_i\frac{\sigma}{\varepsilon} - c\frac{\sigma}{\varepsilon} = -2\,c_i\frac{\sigma}{\varepsilon}$	Eq. (13)
$\int_0^h \frac{1}{r}\frac{\partial}{\partial r}\left(c_i r\frac{\partial\Psi}{\partial r}\right)dz = \frac{1}{r}\frac{\partial}{\partial r}\left(r\int_0^h(\overline{c_i}+\widehat{c_i})\frac{\partial\Psi}{\partial r}\,dz\right)$	Eq. (14)
$= \frac{1}{r}\frac{\partial}{\partial r}\left(r\overline{c_i}\int_0^h\frac{\partial\Psi}{\partial r}\,dz\right) + \frac{1}{r}\frac{\partial}{\partial r}\left(r\int_0^h\widehat{c_i}\frac{\partial\Psi}{\partial r}\,dz\right)$	
$= \frac{h}{r}\frac{\partial}{\partial r}\left(r\overline{c_i}\frac{\partial\overline{\Psi}}{\partial r}\right) + \frac{1}{r}\frac{\partial}{\partial r}\left(r\int_0^h\widehat{c_i}\frac{\partial\Psi}{\partial r}\,dz\right)$	
$\int_0^h \frac{\partial^2 c_i}{\partial z^2}dz = \left(\frac{\partial c_i}{\partial z}\right)_h - \left(\frac{\partial c_i}{\partial z}\right)_0 = 0$	Eq. (15)
$\int_0^h \frac{1}{r}\frac{\partial}{\partial r}\left(r\frac{\partial c_i}{\partial r}\right)dz = \frac{1}{r}\frac{\partial}{\partial r}\left(r\frac{\partial}{\partial r}\right)\int_0^h c_i dz = \frac{1}{r}\frac{\partial}{\partial r}\left(r\frac{\partial\overline{c_i}h}{\partial r}\right)$	Eq. (16)

Table 2
Parameter values used in the model.

Parameter	Value/Range
Relative solvent permittivity, ε_r	80
Ion Diffusivity, D	10^{-9} m^2/s
Temperature, T	298 K
Fluid mass density, ρ	1000 kg/m^3
Fluid viscosity, μ	0.001 Pa.s
Domain radius range, L	20-10000 nm
Domain height, h	4 nm

$$\overline{C_i}(r) = \frac{1}{h}\int_0^h C_i(r,z)dz \tag{9}$$

Table 1 provides the integrated forms of each term in the Poisson and Nernst-Planck equations. For some terms, we have used the top and bottom boundary conditions of the 2D model.

Based on the information provided in Table 1, the final form of the PNP equations in a one-dimensional space may be written as:

$$\frac{1}{r}\frac{\partial}{\partial r}\left(r\frac{\partial\overline{\Psi}h}{\partial r}\right) - 2\,\frac{\sigma}{\varepsilon} = -\frac{h\sum eN_a z_i\overline{c_i}}{\varepsilon} \tag{17}$$

$$\frac{\partial\overline{c_i}h}{\partial t} + \frac{D_i N_a e z_i}{k_B T}\left[\frac{1}{r}\frac{\partial}{\partial r}\left(r\overline{c_i}\frac{\partial\overline{\Psi}h}{\partial r}\right) - 2c_i\,\frac{\sigma}{\varepsilon}\right] + \frac{D_i}{r}\frac{\partial}{\partial r}\left(r\frac{\partial\overline{c_i}h}{\partial r}\right) = 0 \tag{18}$$

In 1D model, the effect of surface charge density should be taken into account. To do so, the second term in the left-hand side of Eq. (17) (*i.e.*, $-2\frac{\sigma}{\varepsilon}$) is defined as a source term. This term originates from integrating the first term of Poisson equation along the height of the aqueous film (Eq. 10). Considering Eqs. (17) and (1), we have defined the charge density in the one-dimensional space as:

$$\rho_e = -\frac{2}{h}\,\sigma + e\,n_a\left(c_p - c_m\right) \tag{19}$$

We have first solved these equations for the initial equilibrium condition and after that we solved them for dynamic condition when we expose the domain to the low salinity bulk fluid.

Table 3
The dimensionless form of some key variables.

Dimensionless variable	Formula
Dimensionless radius, r^*	$\frac{L}{\lambda_D^H}$
Dimensionless height, z^*	$\frac{h}{\lambda_D^H}$
Dimensionless electric potential, Ψ^*	$\frac{e\Psi}{k_B T}$
Dimensionless Concentration, c^*	$\frac{c_i}{c_b^H}$

3.4. Model parameter values

Parameters values considered for our simulations are given in Table 2. In the Nernst-Planck equation, only migration term and the existence of two ion species (c_p and c_m), with valences1.0 and -1.0, were included.

To better present the modelling results, some dimensionless variables are used as defined in Table 3. Here, λ_D^H, is the Debye length for the system under high salinity initial condition determined using $\lambda_D^H = \left(\frac{\varepsilon k_B T}{e^2 n_a \sum z_i^2 c_b^H}\right)^{0.5}$.

4. Simulation results and discussion

In this section, we provide the results obtained from the numerical simulation of coupled PNP equations. We will first describe the results for electrical potential and ion concentrations under initial equilibrium condition obtained from our 1D mode. Afterwards, we compare the dynamic results of this 1D model with those of 2D model to verify our model. To show the efficiency of the developed model, the computational time ratio between the 1D model and the 2D model is provided for different domain lengths (including $r = 1000$, 5000, *and*10000*nm*). The analysis showed that the 1D model can solve the Equations 180–220 times faster than the 2D model. After verification, we use the developed efficient model to perform simulation for a much longer domain size ($r = 0.5mm$) which is not feasible to be simulated using the original 2D model due to its computational demands.

4.1. Initial equilibrium condition for the 1D model

Initially, the domain is filled with high salinity bulk solution which is under equilibrium condition. We performed a simulation for $r^* = 2$ and $z^* = 0.4$ with a constant surface charge density $\sigma = -0.017c/m^2$. Fig. 3

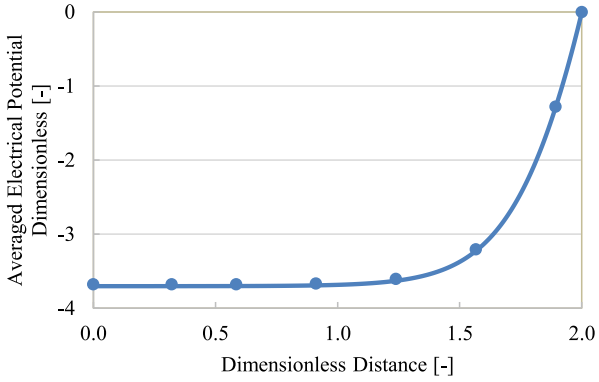

Fig. 3. *Electrical potential.* The initial distribution of electrical potential ($r^* = 2$ and $z^* = 0.4$) with the domain filled with high salinity solution. Solid lines represent the results for the 1D and the markers representing the corresponding results of the 2D models.

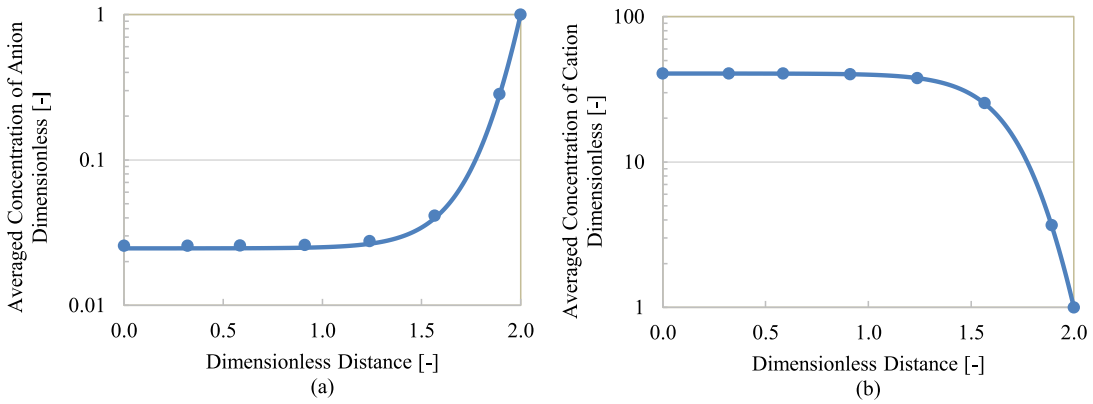

Fig. 4. *Concentration profiles.* Initial distribution of concentration along the domain for (a) anion and (b) cation ($r^* = 2$ and $z^* = 0.4$) with the domain filled with high salinity solution. Solid lines represent the results for the 1D and the markers representing the corresponding results of the 2D models.

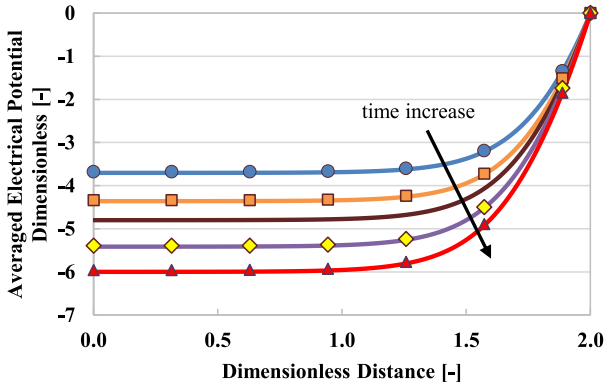

Fig. 5. *Dynamic conditions.* Evolution of electric potential in radial direction ($r^* = 2$ and $z^* = 0.4$). Solid lines represent the results for the 1D and the various markers representing the corresponding results of the 2D models. Blue curve shows the first time step and red curve shows the final equilibrium under low salinity bulk solution. The graphs are equally distributed between the beginning of the simulation and the end time of the simulation corresponding to 10^{-6} seconds.

shows the profile of the electrical potential field along the film radius. It is shown that, moving horizontally away from the centre of the domain ($r^* = 2$), the electrical field becomes weaker. Since the interfaces are negatively charged, the concentration of cation is higher compared to the anion concentration, and by getting closer to the outlet the difference between concentrations become smaller and finally at the outlet the ion concentrations reach to their bulck value. This behaviour is clear in Fig. 4a and b showing the concentration profiles for the anion and cation, respectively. To verify the simulation results for electrical potential and ion concentrations, we compared the results with those obtained using the corresponding 2D model (for $r^* = 2$ and $z^* = 0.4$), that are shown by markers in the following figures.

4.2. 1D model verification under dynamic conditions

To study the system behaviour under dynamic conditions, we performed simulations by including the unsteady, time dependent, terms. To verify the simulation results for electrical potential and ion concentrations, we compared the results with those obtained using the corresponding 2D model (for $r^* = 2$ and $z^* = 0.4$). Fig. 5 shows this comparison for electrical potential evolution over time in radial direction for thin film scenarios. The solid line and the triangular markers show the results that are obtained from 1D and 2D models, respectively. The blue curve shows the results for the first time-step and the red curve shows the final, i.e., equilibrium, solution balanced with the low salinity bulk solution. The simulation run was 10^{-6} seconds, and the graphs are equally distributed between the beginning of the simulation and the end time of the simulation.

Fig. 6a and b show dynamics of anion and cation concentration for thin film, respectively. Again, the solid lines represent the results obtaining from the 1D model and the triangular markers represent those of the 2D models. It is shown that, after we reduce the concentration of surrounding bulk solution, inside the film ions start diffuseing out of the high-salinity solution of the film to the surrounding environment. The

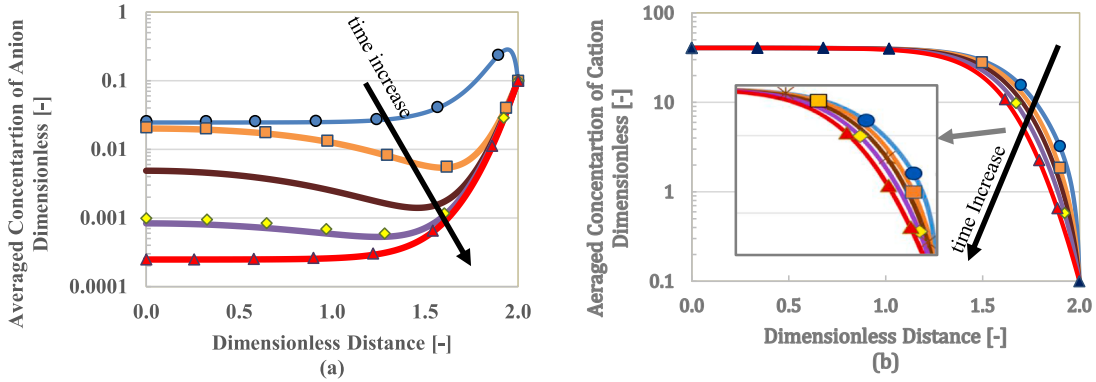

Fig. 6. *dynamic conditions.* Evolution of (a) anion and (b) cation concentration profiles in the radial direction (*fordomain*$r^* = 2$ and $z^* = 0.4$). Solid lines represent the results for the 1D and the various markers representing the corresponding results of the 2D models. Blue curves represent the first time-step after exposing the right boundary to the low salinity bulk solution and the red curves show the final equilibrium under low salinity bulk solution. The graphs are equally distributed between the beginning of the simulation and the end time of the simulation corresponding to 10^{-6} seconds.

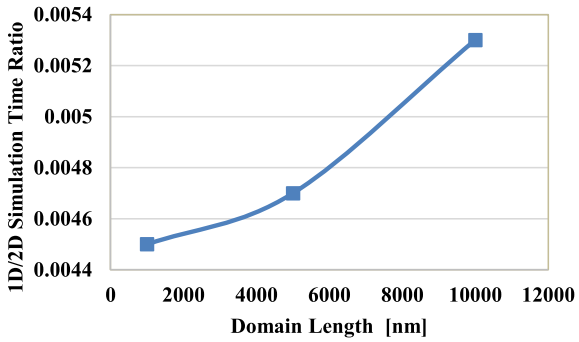

Fig. 7. *Time ratio of 1D over 2D models*. to compare how faster the 1D model could solve the simulation giving the same results as those of the 2D model, we plotted the computational time ratio of 1D over 2D model for different film length.

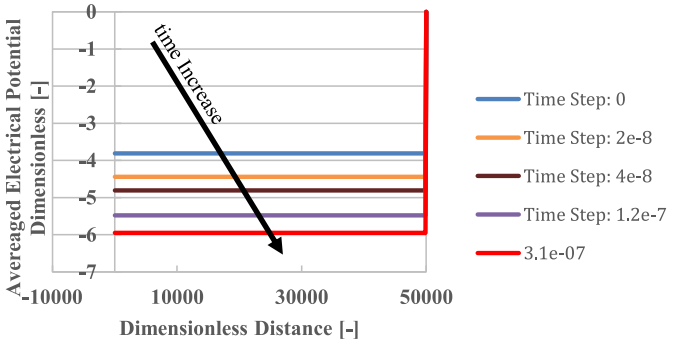

Fig. 8. *Large 1D model*. Evolution of electrical potential under dynamic condition for the film with $r^* = 50000$ and $z^* = 0.4$. Blue curve shows the first time step and the red curve shows the final equilibrium under low salinity bulk solution.

diffusion time is estimated by dividing the squared length of the domain by the diffusion coefficient of ion species.We considered the ions with similar absolute valence and diffusion coefficient but, by comparing Fig. 6a and b you can see the outward diffusion rate of cation is lower compared to anion due to the presence of negative electrical charges on the top and bottom boundaries.

The above figures show exact agreements between the results for electrical potential and ions concentration from both models. The 1D model, however, allows reducing the computational time for over 180-220 times without losing accuracy. Fig. 7 provides the acquired computational benefit using the 1D model for simulations using different film lengths. As demonstrated, the computational benefit becomes much larger for bigger film lengths where the 1D model becomes significantly faster than the 2D model.

4.3. 1D Simulation results for more realistic domain length

We performed simulation using the 1D model for more realistic domain length ($r = 0.5mm$, *i.e.*, 25000 *times largerthan simualtions used for model verifications*) which was not possible to simulate using the 2D model due to the highly computational cost. The results for the electric potential and the anion and cation concentration profile obtained from the 1D model are provided in Fig. 8 and Fig. 9a,b, respectively. The computational time for this large 1D model was 8 min.

Fig. 8 represents the evolution of electric field along the radial direction for this large 1D model. The blue curve shows initial equilibrium condition under high salinity bulk solution and the red curve shows the final equilibrium condition under lower salinity bulk solution. The choice of time steps, as shown in the figure legend, was in some way to better show the evolution of the electrical potential.

In this large 1D model, the negatively charged system was initially under the thermodynamically equilibrium condition for high salinity bulk solution. As we exposed the right boundary to the lower salinity solution, this initial equilibrium condition is disturbed, and the diffusion of ions initiates between high salinity and low salinity bulk solution. Since a field of electrical potential gradient is imposed on the concentration gradient (as explained in Section 3.3.1) the ionic diffusion becomes more limited and due to the presence of negatively electrical charges the mobility of cations is strongly affected and they mostly remain inside the system. Therefore, as shown in Fig. 9a, we could see the diffusion of anion over time while Fig. 9b shows that all the graphs for cation concentration profiles are overlapping each other.

5. Application and future work

Similar to other researchers, we have assumed that the thin film has fixed and rigid boundaries and contains incompressible water. As a result of these assumption, the film thickness remains constant, and no water would flow into or out of the domain. In future works, flow equations should be added to the effective 1D model in order to investigate the spatial and temporal evolution of film thickness due to the coupled effects of electroosmosis and water flow and potential detachment of the oil phase from the solid surface in scales comparable with

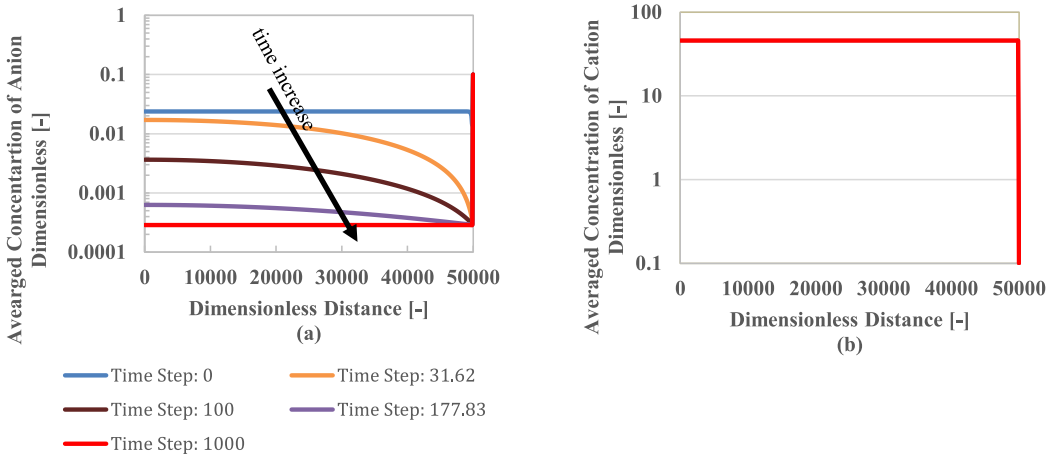

Fig. 9. *Large 1D model*. Evolution of (a) anion and (b) cation concentration profiles in radial direction under dynamic condition for the film with $r^* = 50000$ and $z^* = 0.4$. Blue curve shows the first time step and the red curve shows the final equilibrium under low salinity bulk solution. For cation concentration profiles, all the results overlapping each other due to the presence of negatively electrical charges.

the experimental observations (Mahani, 2015).

Moreover, the electrostatic interface condition in modelling of the solid-fluid interaction is critical as it controls the transport of ions and evolution of disjoining pressure. In a recent study, Pourakaberian et al. (2021) investigated the evolution of hydrodynamic pressure and the electric potential under the effect of ionic strength gradient for different symmetric and asymmetric electrical boundary conditions. Our developed 1D model is valid for symmetric electrical boundary condition of constant charge density as well as in the presence of multi-component solutions and highly overlapping electric double layers. However, for other types of boundary conditions such as constant potential, charge regulation model and asymmetric boundary conditions, appropriate 1D average equations should be derived.

6. Conclusion

In this work, we have developed an effective one-dimensional model to simulate electro-diffusion inside a thin layer of electrolyte located between two charged surfaces. This model has been used to simulate the evolution of electrical potential and ion concentrations distribution along the thin film of electrolyte. Simulations showed that because of the negatively charged surfaces the mobility of the cations was severely affected by the electric charges and these ions had lower outward diffusion rate compared to flux of anions. The developed model could significantly reduce the computational time by a factor of 180-220 compared to simulation using a 2D model. The equivalent 1D model enables solving the nonlinear governing equations for much larger domain lengths providing unique opportunity to simulate experimental results of ion transport in thin films where the very large height to length ratio prevents use of 2D simulations.

Declaration of Competing Interest

None.

Acknowledgements

The authors wish to thank Dr Joost de Graaf for helpful discussions. The second author gratefully acknowledges the support from China Scholarship Council (No. 201609120013). The third author wishes to thank the German Research Foundation (DFG) for supporting this work by funding - EXC2075 – 390740016 under Germany's Excellence Strategy, and acknowledge the support by the Stuttgart Center for Simulation Science (SimTech).

References

Ardenas, A.E.C., Coalson, R.D., Kurnikova, M.G., 2000. Three-dimensional poisson-nernst-planck theory studies: influence of membrane electrostatics on gramicidin a channel conductance. Biophys. J. 79, 80–93.

Alharthy, N.S., Nguyen, T., Kazemi, H., Teklu, T., Graves, R., 2013. Multiphase compositional modeling in small-scale pores of unconventional shale reservoirs. In: *Proceedings of the* SPE 166306 Presented in *SPE Annual Technical Conference and Exhibition* held in New Orleans, Louisiana, 30 September-2 October.

Alizadeh, A., Jin, X., Wang, M., 2019. Pore-scale study of ion transport mechanisms in inhomogeneously charged nanoporous rocks: impacts of interface properties on macroscopic transport. J. Geophys. Res. Solid Earth 124, 5387–5407.

Bazant, M.Z., Kilic, M.S., Storey, B.D., Ajdari, A., 2009. Towards an understanding of induced charge electrokinetics at large applied voltages in concentrated solutions. Adv. Colloid Interface Sci. 152, 48–88.

Brumleve, T.R., Buck, R.P., 1978. Numerical solution of the nernst-planck and poisson equation system with applications to membrane electrochemistry and solid state physics. J. Electroanal. Chem. 90, 1–31.

Chen, J.H., Mehmani, A., Li, B., Georgi, D., Jin, G., 2013. Estimation of total hydrocarbon in the presence of capillary condensation for unconventional shale reservoirs. In: *Proceedings of the* SPE 164468 Presented in *SPE Middle East Oil and Gas Show and Conference* held in Manama. Bahrain, 10-13 March.

Coalson, R.D., Kurnikova, M.G., 2005. Poisson-nernst-planck theory approach to the calculation of current through biological ion channels. IEEE Trans. Nanobiosci. 4, 81–93.

Cohen, H., Cooley, J.W., 1965. The numerical solution of the time-dependent nernst-planck equations. Biophys. J. 5, 145–162.

Corry, B., Kuyucak, S., Chung, S.H., 2003. Dielectric self-energy in poisson-boltzmann and poisson-nernst-planck models of ion channels. Biophys. J. 84, 3594–3606.

Damiani, L.H., Yang, Y., Churakov, S.V., Kosakowski, G., 2015. Nernst-Planck Solver 580 (NPS) Applied to Diffusion of Ions Through a Constricted Pore. CEBAMA, Contract Number: 662147. Deliverable nD4. 13 Draft of the 3rd Annual Project Workshop Proceeding, 309–316.

Du, L., Chu, L., 2012. Understanding anomalous phase behavior in unconventional oil reservors. In: *Proceedings of the*SPE 161830 Presented in *SPE Canadian Unconventional Resource Conference* held in Calgary. Alberta, Canada, 30 October-1 Novembe.

Eisenberg, B., 1998. Ionic channels in biological membranes-electrostatic analysis of a natural nanotube. Contemp. Phys. 39 (6), 447–466.

Eisenman, G., Dani, J.A., 1987. An introduction to molecular architecture and permeability of ion channels. Ann. Rev. *Biophys. Biophys. Chem.* 16, 205–226.

Hille, B., 1978. Ionic channels in excitable membranes. current problems and biophysical approaches. Biophys. J. 22, 283–294.

Hollerbach, U., Chen, D.P., Busath, D.D., Eisenberg, B., 2000. Predicting function from structure using the poisson-nernst-planck equations: sodium current in the gramicidin a channel. Langmuir 79, 5509–5514.

Niasar, V.J., Mahani, H., 2016. Nonmonotonic pressure field induced by ionic diffusion in charged thin films. Ind. Eng. Chem.Res. 55, 6227–6235.

Jiang, G., Wang, P., Chang, C., Li, D., Liu, J.Z., 2014. An equivalent 1D nanochannel model to describe ion transport in multilayered graphene membranes. Prog. Nat. Sci. Mater. Int. 28, 246–250.

Jung, Y.W., Lu, B.Z., Mascagni, M., 2009. A computational study of ion conductance in the KscA K+ channel using a nernst-planck model with explicit resident ions. J. Chem. Phys. 131.

Kelessidis, V.C., 2017. Yield Stress of Bentonite Dispersions. Rheol: open access. 1:101.

Kilic, M.S., Bazant, M.Z., Ajdari, A., 2007. Steric effects in the dynamics of electrolytes at large applied voltages. ii. modified poisson-nernst-planck equations. Phys. Rev. E 75.

Kilic, M.S., Bazant, M.Z., Ajdari, A., 2007. Steric effects in the dynamics of electrolytes at large applied voltages. I. Double-layer charging. Phys. Rev. E 75.

Kirby, B.J., 2010. Micro-and Nanoscale Fluid Mechanics: Transport in Microfluidic Devices. Cambridge University Press, Cambridge.

Kurnikova, M.G., Coalson, R.D., Graf, P., Nitzan, A., 1999. A lattice relaxation algorithm for three dimensional poisson-nernst-planck theory with application to ion transport through the gramicidin a channel. Biophys. J. 76, 642–656.

Liu, R., Yao, S., Shen, Y., 2020. Pore-scale investigation on ion transport and transfer resistance in charged porous media with micro-macro structure. J. Mol. Liq. 320, 114481.

Mahani, H., 2015. Kinetics of low-salinity-flooding effect. SPE J. 20, 8–20.

Mareev, S.A., Nichka, V.S., Butylskii, D.Y., Urtenov, M.K., Pismenskaya, N.D., Apel, P.Y., Nikonenko, V.V., 2016. Chronopotentiometric response of electrically heterogeneous permselective surface: 3D modeling of transition time and experiment. J. Phys. Chem. 120, 13113–13119.

Markowich, P., 1986. The Stationary Semiconductor Device Equation. Springer-Verlag/ Wien, New York.

Mohajeri, A., Narsilio, G.A., Pivonka, P., Smith, D.W., 2010. Numerical estimation of effective diffusion coefficients for charged porous materials based on micro-scale analyses. Comput. Geotechn. 37, 280–287.

Naidu, R., Bolan, N., Kookana, R.S., Tiller, K., 1994. Ionic-strength and ph effects on the sorption of cadmium and the surface charge of soils. Eur. J. Soil Sci. 45, 419–429.

Newman, J., 1991. Electrochemical Systems. Prentice Hall.

Norde, W., Lyklema, J., 1978. The adsorption of human plasma albumin and bovine pancreas ribonuclease at negatively charged polystyrene surfaces: I. Adsorption Isotherms. Effects of charge, ionic strength, and temperature. J. Colloid Interface Sci. 66, 257–265.

Park, H.M., Lee, J.S., Kim, T.W., 2007. Comparison of the nernst–planck model and the poisson–boltzmann model for electroosmotic flows in microchannels. J. Colloid Interface Sci. 15, 731–739.

Pismensky, A.V., Urtenov, M.K., Nikonenko, V.V., Sistat, P., Pismenskaya, N.D., Kovalenko, A.V., 2012. Model and experimental studies of gravitational convection in an electromembrane cell. Russ. J. Electrochem. 48, 756–766.

Pivonka, P., Narsilio, G.A., Li, R., Smith, D.W., Gardiner, B.S., 2009. Electrodiffusive transport in charged porous media: from the particle-level scale to the macroscopic scale using volume averaging. J. Porous Media 12, 101–118.

Pourakaberian, A., Mahani, H., Niasar, V., 2021. The impact of the electrical behavior of oil-brine-rock interfaces on the ionic transport rate in a thin film, hydrodynamic pressure, and low salinity waterflooding effect. J. Colloids Surf. A Physicochem. Eng. Asp. 620.

Pride, S., 1994. Governing equations for coupled electromagnetics and acoustics of porous media. Phys. Rev. 50, 15678–15696.

Revil, A., Pezard, P.A., 1999. Streaming potential in porous media 1. Theory of the zeta potential. J. Geophys. Res. 104, 20021–20031.

Rouston, D., 1990. Bipolar Semiconductor Devices. McGraw-Hill, New York.

Selberherr, S., 1984. Analysis and Simulation of Semiconductor Devices. Springer-Verlag, Wien and New York.
Sun, S., 2019. Darcy-scale phase equilibrium modeling with gravity and capillarity. J. Comput. Phys. 399.
Suopaiarvi, T., 2015. Functionalized Nanocelluloses in Wastewater Treatment Applications. University of OULU Faculty of Technology. Thesis for DoctoralApril.
Trefalt, G., Behrens, S.H., Borkovec, M., 2016. Charge regulation in the electrical double layer: ion adsorption and surface interactions. Langmuir 32, 380–400.
Uzdenova, A., Kovalenko, A., Urtenov, M., Nikonenko, V., 2018. 1D mathematical modelling of non-stationary ion transfer in the diffusion layer adjacent to an ion-exchange membrane in galvanostatic mode. Membrane (Basel) 8, 84.
Zhang, T., Li, Y., Cai, J., Meng, Q., Sun, S., Li, C., 2020. A digital twin for unconventional reservoirs: a multiscale modeling and algorithm to investigate complex mechanisms. Hinduawi Geofluids 2020, 8876153. , 12 pages.
Zhang, T., Li, Y., Sun, S., Bai, H., 2020. Accelerating flash calculations in unconventional reservoirs considering capillary pressure using an optimized deep learning algorithm. J. Petroleum. Sci. Eng. 195.
Zhang, X., Tartakovsky, D.M., 2017. Effective ion diffusion in charged nanoporous materials. J. Electrochem. Soc. 164.
Zheng, Q., Wei, G.W., 2011. Poisson–boltzmann–nernst–planck model. J. Chem. Phys. 134.